


## PAPER

View Article Online  
View Journal | View IssueCite this: *Nanoscale*, 2024, **16**, 18356

# First Cu-nanostar as a sustainable catalyst realized through synergistic effects of bowl-shaped features and surface activation of sporopollenin exine†

 Vijayendran Gowri,<sup>‡a,b</sup> Sarita Kumari,<sup>‡a</sup> Raina Sharma,<sup>a</sup> Abdul Selim<sup>a</sup> and Govindasamy Jayamurugan <sup>\*a</sup>

Recently, nanostar-shaped structures, including gold nanostars (NS), have drawn much attention for their potential use in surface-enhanced Raman spectroscopy (SERS) and catalysis. Yet, very few studies have been conducted on Cu–Au hybrid NS, and there are none for Cu-based NS. Herein, we describe an effective method for controlling copper-oxide nanostar (ESP-PEI-Cu<sup>I/II</sup>O-NS) growth using sporopollenin as a sustainable template material. However, ESP-PEI-Cu<sup>I/II</sup>O-NS growth depends on sporopollenin surface functionalization. Sporopollenin surface activation was done by amine functionalization with polyethyleneimine (PEI), without which ESP-PEI-Cu<sup>I/II</sup>O-NS growth was not observed. The sporopollenin's exine (outer wall) has a bowl-like structure, which mediates the growth of Cu nanorods, resulting in an NS morphology. Furthermore, due to their increased surface area, ESP-PEI-Cu<sup>I/II</sup>O-NS showed excellent catalytic activity for Huisgen 1,3-dipolar cycloadditions even when used in H<sub>2</sub>O and without additives under green conditions. This approach utilising biomass as a sustainable template would pave the way for developing controlled growth of nanostructures for SERS-related and catalytic applications.

Received 12th March 2024,  
Accepted 15th August 2024

DOI: 10.1039/d4nr00390j

rsc.li/nanoscale

## Introduction

In today's era of global warming and environmental degradation, there is a strong focus on replacing harmful chemicals with eco-friendly alternatives and sustainable chemistry practices.<sup>1,2</sup> Copper-oxide nanostructured materials are a fast-developing class due to their excellent physical and chemical properties arising due to their size of 1 to 100 nanometres (nm) and the variety of shapes they take.<sup>3,4</sup> They are ideal candidates for applications such as environmental remediation,<sup>5</sup> energy storage,<sup>6</sup> nanophotonics,<sup>7</sup> plasmonics,<sup>8–11</sup> catalysis,<sup>12,13</sup> and nanoscale electronics.<sup>14</sup> According to many studies, size and shape (morphology) can influence nanostructured materials' activity due to their high surface-to-volume ratio and active sites exposed in specific phases.<sup>15</sup> Given the

challenges in controlling these parameters, research has shifted towards regulating their morphology, size and shape because slight variations in factors such as reaction conditions, temperatures, electrostatic interactions, and steric confinement can significantly alter the materials' properties.<sup>16</sup> The preparation of Cu<sup>I/II</sup>O-NPs with diverse sizes and shapes has been carried out *via* a wide range of methods, including sonochemistry, alcoholothermal synthesis, thermal decomposition by direct heating, electrochemistry, and colloid-thermal synthesis with microwave radiation.<sup>17</sup> The methods described above have been demonstrated to be able to produce nanostructured Cu<sub>x</sub>O in a wide range of morphologies, such as nanocrystals, nanotubes, nano-dendrites, nanorings, nanowires, nanorods, nanoribbons, microspheres, and macro whiskers along with several other morphologies.<sup>18,19</sup>

From a sustainable chemistry point of view, plant waste, especially sporopollenin, is a potential precursor in various applications primarily explored as a nanocarrier for drugs,<sup>20</sup> pesticide carriers,<sup>21</sup> and food additives.<sup>22</sup> However, the unique feature of sporopollenin (SP) being a rugged (resistant to chemical, light, and biological degradation) material<sup>23</sup> and its nanosized (typically, this ranges from tens to hundreds of nanometers, depending on the origin of the species)<sup>20</sup> bowl-like surfaces with channel pores make it an excellent candidate for use in catalysis as a sustainable heterogeneous catalyst/

<sup>a</sup>Institute of Nano Science and Technology, Knowledge City, Sector 81, Mohali, Punjab 140306, India. E-mail: jayamurugan@inst.ac.in, jayamuruganinst@gmail.com

<sup>b</sup>Gowriz Skincare Pvt Ltd incubated at Technology Business Incubator (TBI) at IISER Mohali, Knowledge City, Sector 81, Mohali, Punjab 140306, India

†Electronic supplementary information (ESI) available: General information and instrumentation, an experimental section, characterization of the catalyst, and spectral details of products. See DOI: <https://doi.org/10.1039/d4nr00390j>

‡These authors contributed equally to this work.

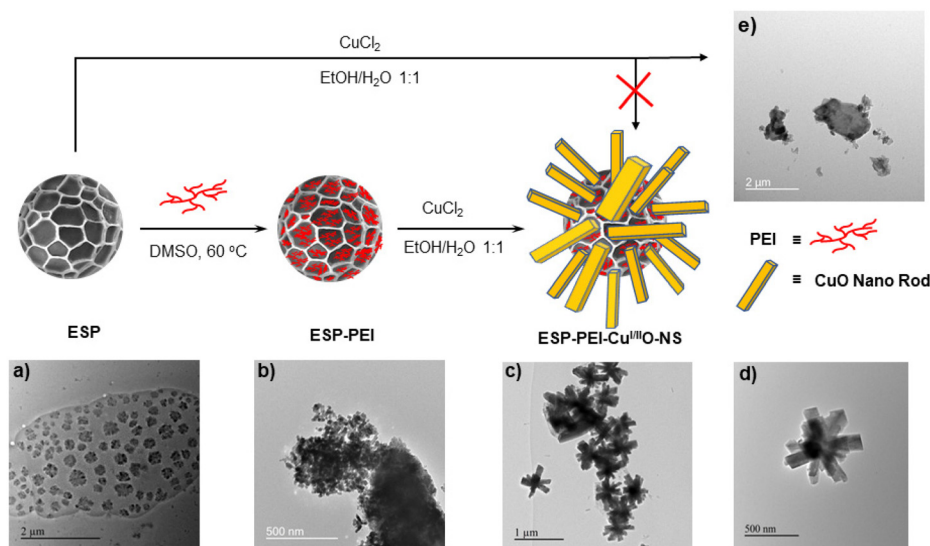
support for easy recoverability and reuse.<sup>24</sup> We envisage that this feature can be utilised as a template to synthesize particular nanosized shapes, for example an unexplored nanostar like “morning star weapon”.<sup>25</sup> There are metal nanoparticles shaped like the “morning star” especially gold nanoparticles<sup>26–29</sup> and rarely hybrids (Ag and Cu with gold)<sup>30–34</sup> composed of a central sphere surrounded by points. This research has mainly been related to gold nanoparticles that can concentrate electromagnetic fields at their extremities. While many shapes of copper oxide have been reported, to the best of our knowledge, the nanostar has not been reported.

Sporopollenin (SP) is a highly cross-linked biological polymer available in large quantities naturally from plant-based biomass, which can be utilised in the circular economy. It is a chemically inert major component of the tough outer (exine) walls of plant spores and pollen grains and is composed of elements such as carbon, hydrogen, and oxygen. Because of its unique features, such as cytocompatibility,<sup>35</sup> large cavities for drug cargo, and a tough protecting layer, SP is being researched heavily in drug delivery,<sup>36</sup> besides other applications.<sup>37</sup> However, its application in catalysis is still at an infant stage.<sup>38</sup> While the exact basic monomeric unit structure of sporopollenin is still under investigation and debatable, many studies have suggested that it is composed of aliphatic-polyketide-derived polyvinyl alcohol units and 7-*O*-*p*-coumaroylated C16 aliphatic units, crosslinked through a distinctive dioxane moiety featuring functional groups such as hydroxyl, epoxide, acetal, *etc.*<sup>39</sup> Thus, in this work, we envisaged that the unique surface profile with bowl-like compartmentalization lycopodium clavatum (LC) based spores would act as a template to grow nanorods, which may result in the synthesis of a nanostar-like copper-oxide catalyst with higher activity. Notably, results revealed that the growth of copper-oxide rods on the spore's

surface depends mainly on the surface functionalization with polyamines, without which nanostar growth has not been observed. Furthermore, its catalytic activity was investigated against copper(i)-catalyzed azide-alkyne cycloadditions (CuAAC) under environmentally benign conditions.

## Results and discussion

While various shapes of exine sporopollenin are available, lycopodium clavatum (LC) was chosen as the template material due to its unique surface shape, characterized by bowl-like irregular hexagons. This shape may facilitate the nucleation of rod-shaped nanoparticles, leading to the formation of copper-oxide ( $\text{Cu}^{\text{II}}\text{O}$ ) nanostar-shaped catalysts, which could result in improved catalytic activity, even when using water as a solvent and at room temperature.<sup>40</sup> With this hypothesis for synthesizing a copper-oxide ( $\text{Cu}^{\text{II}}\text{O}$ ) nanostar-shaped nanostructure, we have performed the synthesis with lycopodium powder (Section B, ESI†). However, to remove the genetic and other associated materials and to obtain empty sporopollenin (ESP) (Scheme 1a) with a hollow morphology, the established literature procedure was adopted using the phosphoric acid treatment method (for experimental details, see Section B, ESI†).<sup>41</sup> Preliminary investigation of ESP for the copper-oxide synthesis using  $\text{CuCl}_2$  in EtOH/ $\text{H}_2\text{O}$  1:1 did not provide nanostars (Scheme 1e). This experiment suggests that nascent surface functional groups don't initiate nucleation for the nanostar growth because of the C-, H-, and O-based non-coordinating functional groups. Therefore, we envisaged covalently functionalizing polyethylene imine (PEI) to create coordinating nitrogen/amine functionalities. This may occur due to the presence of epoxide, alcohol, and aldehyde that may facilitate nuclea-



**Scheme 1** Synthetic route to the ESP-templated  $\text{Cu}^{\text{II}}\text{O}$  nanostar; TEM image of (a) sporopollenin without the genetic material (ESP), (b) PEI coated ESP (ESP-PEI), (c) copper-oxide nanostars (ESP-PEI- $\text{Cu}^{\text{II}}\text{O}$ -NS), (d) zoomed image of copper-oxide nanostars (ESP-PEI- $\text{Cu}^{\text{II}}\text{O}$ -NS), and (e) PEI-unfunctionalized ESP- $\text{Cu}^{\text{II}}\text{O}$ .

tion on the ESP. To test this hypothesis, we have executed the amine functionalization using PEI (Mw 750 000 Daltons, 50 wt% in H<sub>2</sub>O, Sigma Aldrich) in DMSO solvent at 60 °C to obtain ESP-PEI (Scheme 1b). After amine functionalization, upon treatment with CuCl<sub>2</sub> in EtOH/H<sub>2</sub>O 1 : 1, a copper-oxide nanostar (ESP-PEI-Cu<sup>I/II</sup>O-NS) was yielded (Scheme 1c and d).

The Fourier transform infrared (FT-IR) spectroscopy study was investigated to shed light on the cleaning of spores and PEI-functionalization (Fig. 1a). The FT-IR spectrum of the ESP showed the absence of a peak at 665 cm<sup>-1</sup> and 80 cm<sup>-1</sup> shifts in C–O–C (1092 cm<sup>-1</sup>) in comparison with SP due to the removal of genetic materials and the presence of epoxide groups on the sporopollenin surface, respectively, whereas the FT-IR spectrum of ESP-PEI showed several new peaks at 3160 (N–H, m), 3428 (O–H, m), 1654 (N–H bend, m), 1117 (C–O–C of ESP, s), 807 (m), and 671 (m) cm<sup>-1</sup> characteristic of PEI and ESP. They indicated efficient PEI coating on the sporopollenin surface *via* covalent amine functionalization with the epoxide-generating aminol groups. Similarly, the FT-IR spectrum of ESP-PEI-Cu<sup>I/II</sup>O-NS showed the growth of Cu<sup>I/II</sup>O-NS and its interaction with amine functional groups, which is evident from its significant shift in the N–H peaks at 3280 cm<sup>-1</sup>, while peaks such as 1655 and 804 cm<sup>-1</sup> did not exhibit a significant shift. These results indicate that the covalent functionalization of PEI on the spore helps in the growth of copper-oxide nanorods due to the presence of multiple *N*-chelating sites, activating the growth of copper-oxide nanorods.

The spores' size, shape, and morphology were analyzed by transmission electron microscopy (TEM) analysis. The TEM images of ESP showed that they were evenly distributed and spherical, and the particle size distribution was in the range of 100–300 nm (Scheme 1a), which is quite smaller-sized ESP as typically the reported sporopollenin size is in the range of >1 μm. Notably, the microscopic analysis requires optimization for better reproducibility by manipulating the power source due to smaller particles, whereas the TEM image of ESP-PEI shows aggregated densely packed structures upon coating of PEI over sporopollenin (Scheme 1b). However, the growth of copper oxide over the ESP afforded uniformly distributed “morning star” kind of morphology, and the particle size distribution of the formed ESP-PEI-Cu<sup>I/II</sup>O-NS was found to be around 500–750 nm (Scheme 1c). However, in the case of sporopollenin, having no PEI functionalization after the treatment with CuCl<sub>2</sub> showed no nanostar. Instead, it showed clusters (Scheme 1e), indicating that PEI has been acting as a chelating agent, mediating the growth of copper-oxide nanorods over the sporopollenin capsules. After the successful synthesis of morning star-shaped particles, the elemental composition was investigated by energy-dispersive X-ray analysis (EDAX), powder X-ray Diffraction (PXRD), X-ray photoelectron spectroscopy (XPS), and inductively coupled plasma-mass spectrometry (ICP-MS) analyses. TEM-EDAX elemental mapping showed the presence of elements C, O, N, Cl, and Cu due to PEI and CuO (Section C, Fig. S2, S3 and Table S1, ESI†). The

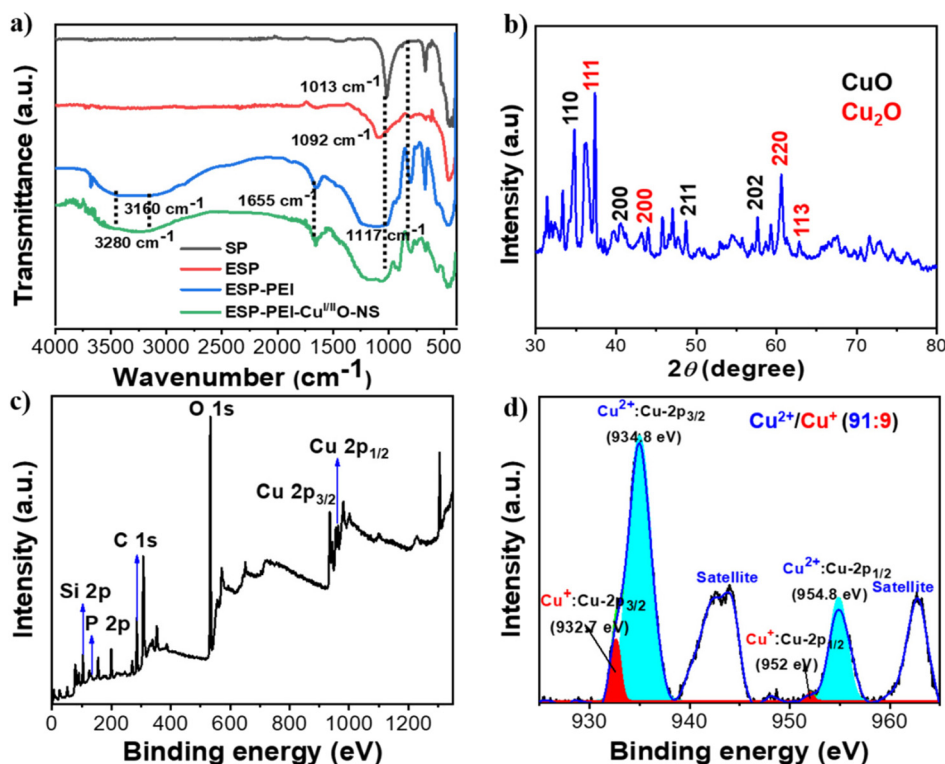


Fig. 1 (a) Overlapped FT-IR spectra of SP, ESP, ESP-PEI, and ESP-PEI-Cu<sup>I/II</sup>O-NS, (b) PXRD pattern of ESP-PEI-Cu<sup>I/II</sup>O-NS, (c) XPS spectra of ESP-PEI-Cu<sup>I/II</sup>O-NS, and (d) high-resolution XPS-survey spectra of Cu<sup>I/II</sup> NPs of the copper 2p profile of the ESP-PEI-Cu<sup>I/II</sup>O-NS catalyst.

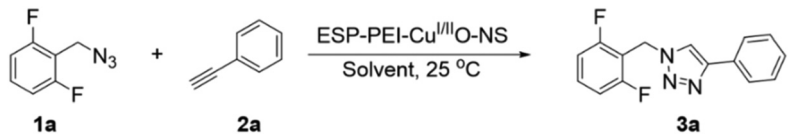
high resolution TEM image clearly shows metallic fringes (0.392 nm) on the nanorods without any organic coating (Fig. S2b, ESI†). This observation is further supported by EDX mapping of different elements, such as carbon (organic component) and Cu (CuO). The mapping shows no nanostar feature for carbon, while a nanostar feature is observed for Cu. This suggests the absence of an organic component on the nanorods, except at the core of the nanostar. Therefore, based on the HR-TEM and EDX mapping data, we infer that the nanorods are entirely composed of CuO, originated from the organic ESP template and are not coated or encapsulated by the organic ESP template.

Furthermore, the oxidation and crystalline state of Cu were analyzed by powder XRD, which indicates the monoclinic structure of CuO and the cubic fcc structure of Cu<sub>2</sub>O (Fig. 1b). The observed diffraction peaks at (111), (200), (211), (220), and (113) reflections are of the standard fcc cuprite crystal structure. This suggests the formation of ESP-PEI-Cu<sup>I/II</sup>O-NS. The unassigned peaks might be due to the precursors as observed by the overlapped XRD spectra of ESP, ESP-PEI, and ESP-PEI-Cu<sup>I/II</sup>O-NS (Fig. S6, ESI†). Furthermore, (XPS) survey (Fig. 1c) of the prepared ESP-PEI-Cu<sup>I/II</sup>O-NS showed the presence of Si, P, C, O, and Cu elements. The deconvoluted spectra of Cu indicated the presence of CuO/Cu<sub>2</sub>O in a ratio of 91 : 9. The characteristic binding energy corresponding to Cu 2p<sub>3/2</sub> of copper(I) has exhibited a weak peak at 933 eV. In the case of copper(II), a strong peak has appeared at 935.4 eV, which is characteristic binding energy for the Cu 2p<sub>3/2</sub>. The thermal stability of the catalyst studied by thermogravimetric analysis (TGA), both ESP-PEI and ESP-PEI-Cu<sup>I/II</sup>O-NS, showed excellent thermal stability with a total weight loss of 14.5 and 23.8%, respectively, up to 800 °C (Section C and Fig. S4, ESI†). The initial stage weight loss up to 200 °C occurs presumably due to the removal of absorbed ethanol and water from the catalyst. Further weight loss in the temperature range of 200 to 800 °C is attributed to the degradation of PEI. Furthermore, the loading of copper on ESP-PEI-Cu<sup>I/II</sup>O-NS was found to be

12.82 wt%, as determined by inductively coupled plasma mass spectrometry (ICP-MS). It is clear from these results that PEI acts as a reducing metal ion and stabilising agent for nanorod growth. In addition, solid-state ultraviolet-visible (UV/Vis) spectra were also obtained for ESP, ESP-PEI and ESP-PEI-Cu<sup>I/II</sup>O-NS to understand how the optical properties of ESP have been modified upon functionalization with the PEI polymer and deposition of CuO nanorods. In the comparative diffuse UV/Vis reflectance spectra, ESP has demonstrated a single absorption band ranging from 230–355 nm with  $\lambda_{\text{max}}$  = 263 nm (Fig. S5, ESI†), whereas ESP-PEI showed a significant bathochromic shift of the absorption band ranging 234–543 nm with  $\lambda_{\text{max}}$  = 263 nm indicating successful amine functionalization. Interestingly, ESP-PEI-Cu<sup>I/II</sup>O-NS exhibits two absorption bands ranging from 230–388 and 400–619 nm, with  $\lambda_{\text{max}}$  values at 276 and 499 nm, respectively. These bands are likely due to charge transfer transitions from O<sub>2</sub><sup>−</sup>(2p) → Cu<sup>2+</sup>(3d) and Cu<sup>2+</sup>–O<sub>2</sub><sup>−</sup>–Cu<sup>2+</sup>, as well as d–d transitions of Cu<sup>2+</sup> with various symmetries.<sup>42</sup> A similar absorption profile has been previously observed for CuO nanoflower structures, showing absorption wavelengths up to 780 nm.<sup>42</sup> The lower end of the absorption band (619 nm) may be attributed to coordination with the amine polymer.

After the successful synthesis and characterization of sporopollenin templated Cu<sup>I/II</sup>O nanostars (ESP-PEI-Cu<sup>I/II</sup>O-NS), as originally intended, we then evaluated their catalytic activity to promote the Huisgen 1,3-dipolar cycloaddition reaction. For this purpose, 2,6-difluoro-benzyl azide and phenylacetylene were chosen as substrates for the model reaction. Initially, the reaction was carried out by varying the solvents at room temperature (25 °C) (Table 1). MeOH and MeOH/H<sub>2</sub>O (1 : 1, v/v) showed conversion of 50 and 90%, respectively (Table 1 entries 3 and 6). Despite increasing the reaction time to 48 h, no complete conversion was observed. Surprisingly, full conversion was obtained after 24 h for **3a** (1-(2,6-difluorobenzyl)-4-phenyl-1H-1,2,3-triazole) with an isolated yield of 98.4% only in the case of H<sub>2</sub>O as the solvent (Table 1, entry 7).

**Table 1** Optimization of reaction conditions for the azide–alkyne cycloaddition reaction (CuAAC)<sup>a</sup>

			
S. no.	Solvent	Time (h)	Conversion <b>3a</b> <sup>b</sup> (%)
1	CH <sub>3</sub> CN	24	—
2	CHCl <sub>3</sub>	24	—
3	MeOH	48	50
4	EtOH	24	—
5	i-PrOH	24	—
6	MeOH/H <sub>2</sub> O 1 : 1	30	90
7	H <sub>2</sub> O	24	100
8	Toluene	24	—

<sup>a</sup> Reaction conditions: 2,6-difluoro-benzylazide **1a** (0.059 mmol, 1 equiv.), phenylacetylene **2a** (0.059 mmol, 1 equiv.), solvent (1 mL), ESP-PEI-Cu<sup>I/II</sup>O-NS (3.4 mol%), 25 °C. <sup>b</sup> Conversion was determined by GC-MS.

Table 2 Substrate scope for CuAAc

$  \begin{array}{c}  \text{R}_1\text{-N}_3 + \text{HC}\equiv\text{C-R}_2 \xrightarrow[\text{H}_2\text{O, 25 }^\circ\text{C}]{\text{ESP-PEI-Cu}^{\text{III}}\text{O-NS}} \text{R}_1\text{-N=N-C(R}_2\text{)=N} \\  \text{1 (a-c)} \qquad \text{2 (a-f)} \qquad \qquad \qquad \text{3 (a-n)}  \end{array}  $				
S. no.	Substrate		Time (h)	Isolated yield 3(a-n) (%)
	R <sub>1</sub> 1(a-c)	R <sub>2</sub> 2(a-f)		
1			24	3a (98.4)
2			48	3b (91)
3			36	3c (86)
4			36	3d (98.6)
5			24	3e (94.8)
6			48	3f (76.3)
7			40	3g (92.9)
8			30	3h (80.4)
9			24	3i (95.6)



Table 2 (Contd.)

$R_1-N_3 + \text{R}_2 \xrightarrow[H_2O, 25^\circ C]{ESP-PEI-Cu^{III}O-NS} R_1-N=N-N(R_2)$				
	1 (a-c)	2 (a-f)	3 (a-n)	
S. no.	Substrate			
10			26	3j (97.3)
11			48	3k (87.3)
12			30	3l (90.8)
13			24	3m (90.4)
14			30	3n (91.5)

Reaction conditions: **1(a-c)** (1 equiv.), **2(a-f)** (1 equiv.), H<sub>2</sub>O (1 mL), ESP-PEI-Cu<sup>III</sup>O-NS (3.4 mol%), 25 °C.

Furthermore, exclusively a 1,4 regio-isomer was formed by the catalytic reaction as indicated by NMR (Section D(iii), ESI†). Also, no cycloaddition product was observed in the case of any other solvents we tested so far. Therefore, H<sub>2</sub>O was chosen as the optimal solvent for the rest of the studies, providing environmentally friendly conditions, as H<sub>2</sub>O is a green solvent.

Furthermore, various substituted azides and alkynes were taken to check the scope of the catalyst for the CuAAC reaction. The azides **1(a-c)** were synthesized *via* already reported procedures, while all the alkynes were purchased commercially (Section D, ESI†). Complete conversion was observed in all the cases, with a good to excellent isolated yield of 76–98% with excellent 1,4 regioselectivity for the triazole products (Table 2). All the products were well characterised by <sup>1</sup>H-, <sup>13</sup>C-NMR spectroscopy and gas chromatography-mass spectrometry (GC-MS) (Section D, ESI†).

After successful substrate scope studies, a reusability study was also conducted under the optimised conditions with the 2,6-difluorobenzyl azide **1a** and the phenylacetylene **2a** to check the sustainability of the catalyst. As soon as the reaction is completed, product **3a** and the catalyst can easily be isolated by solvent extraction with CH<sub>2</sub>Cl<sub>2</sub> and H<sub>2</sub>O, respectively. The organic layer is then dried over Na<sub>2</sub>SO<sub>4</sub>, while the aqueous layer is centrifuged, washed with EtOH three times, and dried

in a vacuum oven to recover the catalyst. This process was repeated up to 5 cycles, but after each cycle, the product yield decreased (Fig. 2, an isolated yield of 98 to 60% in the 5th cycle). The reduction in yields was because of the leaching of

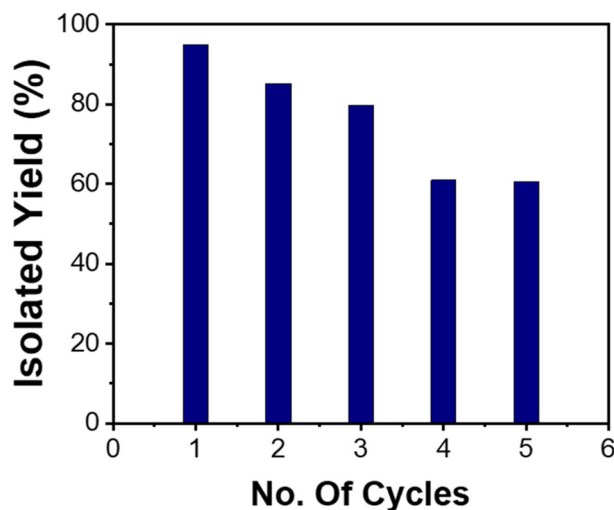


Fig. 2 Isolated yields of **3a** using the ESP-PEI-Cu<sup>III</sup>O-NS catalyst up to five cycles.

**Table 3** Literature comparison for CuAAC reactions in water catalyzed by template supported copper-based catalysts

Entry	Catalyst	Conditions	Temp. (°C)	Catalyst loading (additive)	Time (h)	Yield (%)	Ref.
1	ESP-PEI-Cu <sup>I/III</sup> O-NS	H <sub>2</sub> O	rt	3.4 mol%	24–48	76–98	This work
2	Copper(i)-chelated cross-linked cyclen micelles	H <sub>2</sub> O, N <sub>2</sub>	35	20 ppm	24	80–99	43
3	Nano ferrite-glutathione-copper catalyst	H <sub>2</sub> O, microw.	120	100 mg	0.16	80–99	44
4	Polydiacetylene micelle encapsulated copper nanoparticles	H <sub>2</sub> O	rt	0.35 mol%	24	85–99	45
5	Copper-containing metal-organic nanoparticles	H <sub>2</sub> O	50	5–30 ppm (sodium ascorbate)	24	83–99	46
6	Amphiphilic resin-supported copper catalyst	H <sub>2</sub> O, N <sub>2</sub>	25	5 mol% (sodium ascorbate)	12	85–100	47
7	Copper-doped functionalized $\beta$ -cyclodextrin	H <sub>2</sub> O, N <sub>2</sub>	rt–70	10 mol%	1–12	77–92	48
8	Aminomethyl polystyrene supported copper(i) Cu(i)-AMPS	H <sub>2</sub> O	rt	1 mol%	1–2	43–88	49
9	Activated carbon supported copper	H <sub>2</sub> O	rt	0.5 mol%	6	60–91	50
10	Copper-incorporated porous organic polymer	H <sub>2</sub> O	50	1 mol%	1–12	38–99	51
11	Cellulose acetate-supported copper	H <sub>2</sub> O	rt	5 mol%	8	90–98	52
12	Polystyrene resin-supported CuI-cryptand 22 complex	H <sub>2</sub> O	rt	0.3 mol%	10	78–99	53
13	Cu(ii)-cellulose-poly(hydroxamic acid)	H <sub>2</sub> O	70	0.05 mol% (sodium ascorbate)	3.5	89–96	54
14	Cu(OAc) <sub>2</sub> -SBA-15-PTAA	H <sub>2</sub> O	50	2 mol%	6–12	91–98	55

the Cu from the ESP-PEI-Cu<sup>I/III</sup>O-NS, which is indicated by ICP-MS as the amount of Cu was found to be 8.65% after the 5<sup>th</sup> cycle, *i.e.* 4.17% decrease in the Cu amount, which causes a loss in the catalytic activity. The copper-oxide nanorods are highly exposed on the outside surface, which is the reason for the leaching of Cu from ESP-PEI-Cu<sup>I/III</sup>O-NS as indicated by TEM (Section C, Fig. S8, ESI†). Additionally, we have performed characterization of the recovered catalyst to determine whether metal leaching causes changes in the oxidation states of Cu<sup>I/III</sup>O-NS. For this purpose, XPS analysis was conducted after the fifth cycle of the model reaction. The XPS results showed a change in the Cu<sup>2+</sup>/Cu<sup>+</sup> ratio from 91 : 9 to 73 : 27, presumably due to the leaching of copper ions, which affects the ion ratio and, consequently, the catalytic activity. To ensure that the catalytic activity indeed occurs on the Cu<sup>I/III</sup>O nanostructures and not due to the leaching of the catalyst, we performed a time-dependent reaction profile and monitored the product yield by <sup>1</sup>H-NMR and Cu-release by ICP-MS (for experimental details, see Section C, ESI†). Fig. S7† shows the product yield as well as the percentage of copper release *versus* reaction time profile. The study reveals that the maximum release of copper is 11% between 0–6 h, with a product yield of 36%. However, from 6–24 h, the maximum release increases to 14%, with a product yield of 99%. This suggests that the predominant catalytic activity occurs mainly from the unreleased ESP-PEI-Cu<sup>I/III</sup>O-NS rather than the released ions. Overall, the reaction is very easy to perform; it does not demand any heating or additives with easy separation of compounds, and the catalyst activity within water suggests that it may be suitable for other organic transformation reactions.

The ESP-PEI-Cu<sup>I/III</sup>O-NS catalytic system was compared with other reported template-supported copper-based catalysts which are used in water in order to determine its catalytic performance. In general, the previous work presented in Table 3 shows some limitations, such as the use of additional reducing agents, high temperatures (including some microwave conditions), and inert reaction conditions. In contrast, the current

catalyst, ESP-PEI-Cu<sup>I/III</sup>O-NS, operates efficiently under milder reaction conditions (room temperature, air) without requiring additives. Furthermore, while certain catalysts rely on costly starting materials, we utilized sporopollenin, an abundantly available and cost-effective biopolymer, for catalyst synthesis.

## Conclusion

In the present work, we have demonstrated the unprecedented synthesis of copper-oxide nanostars using sporopollenin exine (ESP) as a sustainable template material. This study unraveled that the synergistic effect of bowl-shaped features and amine functionalization is crucial for the successful growth of nano-star-shaped uniformly sized particles. Furthermore, ESP-PEI-Cu<sup>I/III</sup>O-NS was well characterised using microscopic and other characterization techniques. As analyzed using TEM images, a uniform size of 500–750 nm was observed for the ESP-PEI-Cu<sup>I/III</sup>O-NS. Furthermore, for the first time, Cu<sup>I/III</sup>O NS were tested for their catalytic activity towards the CuAAC reaction and excellent performance was observed with 1,4-regio-selectivity in H<sub>2</sub>O under greener conditions without any additives. We believe this work will open a new window for future studies toward designing “morning star” like nanostructures and their role in catalysis and other areas.

Preprints of this work have been deposited on 17<sup>th</sup> January 2024.<sup>56</sup>

## Author contributions

G. J. conceived the overall project and supervised the effort. V. G. designed the experiments, ran the synthetic protocols, and characterized the catalyst. S. K. designed and ran the experiments related to catalytic application. R. S. and A. S. helped in data curation. V. G. and S. K. wrote the paper together with G. J. with the help from all the authors.

## Data availability

The data supporting this article have been included as part of the ESI.†

## Conflicts of interest

G.J. and V.G. declare a significant financial interest in Gowriz Skincare Pvt Ltd, the company that commercialized the previous sporopollenin synthesis for skin care applications.

## Acknowledgements

This work was supported by the SERB, Department of Science and Technology (DST), grant no. CRG/2022/007139 and SB/S2/RJN-047/2015. G.J. thanks DST-SERB for the Ramanujan Fellowship. S.K. thanks CSIR, India for a Junior Research Fellowship. This article is dedicated to Professor N. Jayaraman on the occasion of his 60<sup>th</sup> birthday.

## References

- 1 R. A. Sheldon, *Green Chem.*, 2016, **18**, 3180–3183.
- 2 M. K. M. Lane, H. E. Rudel, J. A. Wilson, H. C. Erythropel, A. Backhaus, E. B. Gilcher and J. B. Zimmerman, *Nat. Sustain.*, 2023, **6**, 502–512.
- 3 M. B. Gawande, A. Goswami, F. X. Felpin, T. Asefa, X. Huang, R. Silva, X. Zou, R. Zboril and R. S. Varma, *Chem. Rev.*, 2016, **116**, 3722–3811.
- 4 N. Verma and N. Kumar, *ACS Biomater. Sci. Eng.*, 2019, **5**, 1170–1188.
- 5 E. Y. Shaba, J. O. Jacob, J. O. Tijani and M. A. T. Suleiman, *Appl. Water Sci.*, 2021, **11**, 1–41.
- 6 S. M. Cha, G. Nagara, S. C. Sekhar and J. S. Yu, *J. Mater. Chem. A*, 2017, **5**, 2224–2234.
- 7 T. K. Kim, B. VanSaders, J. Moon, T. Kim, C. H. Liu, J. Khamwannah, D. Chun, D. Choi, A. Kargar, R. Che and Z. Liu, *Nano Energy*, 2015, **11**, 247–259.
- 8 D. Garoli, H. Yamazaki, N. Maccaferri and M. Wanunu, *Nano Lett.*, 2019, **19**, 7553–7562.
- 9 B. Serrano-Montes, J. Langer, M. Henriksen-Lacey, D. J. de Aberasturi, D. M. Solis, J. M. Taboada, F. Obelleiro, K. Sentosun, S. Bals, A. Bekdemir, F. Stellacci and L. M. Liz-Marzán, *J. Phys. Chem. C*, 2016, **120**, 20860–20868.
- 10 X. Deng, S. Liang, X. Cai, S. Huang, Z. Cheng, Y. Shi, M. Pang, P. Ma and J. Lin, *Nano Lett.*, 2019, **19**, 6772–6780.
- 11 B. Muzzi, M. Albino, A. Gabbani, A. Omelyanchik, E. Kozenkova, M. Petrecca, C. Innocenti, E. Balica, A. Lavacchi, F. Scavone, C. Anceschi, G. Petrucci, A. Ibarra, A. Laurenzana, F. Pineider, V. Rodionova and C. Sangregorio, *ACS Appl. Mater. Interfaces*, 2022, **14**, 29087–29098.
- 12 A. Selim, K. M. Neethu, V. Gowri, S. Sartaliya, S. Kaur and G. Jayamurugan, *Asian J. Org. Chem.*, 2021, **10**, 3428–3433.
- 13 R. Chopra, M. Kumar and V. Bhalla, *Green Chem.*, 2019, **21**, 3666–3674.
- 14 I. Concina, Z. H. Ibupoto and A. Vomiero, *Adv. Energy Mater.*, 2017, **7**, 1700706.
- 15 S. Mitchell, R. Qin, N. Zheng and J. P. Ramírez, *Nat. Nanotechnol.*, 2021, **16**, 129–139.
- 16 M. Suleiman, M. Mousa, A. Hussein, B. Hammouti, T. B. Hadda and I. Warad, *J. Mater. Environ. Sci.*, 2013, **4**, 792–797.
- 17 K. Nithya, P. Yuvasree, N. Neelakandeswari, N. Rajasekaran, K. Uthayarani, M. Chitra and S. S. Kumar, *Int. J. ChemTech Res.*, 2014, **6**, 2220–2222.
- 18 P. Lignier, R. Bellabarba and R. P. Tooze, *Chem. Soc. Rev.*, 2012, **41**, 1708–1720.
- 19 H. Wang, M. G. Potroz, J. A. Jackman, B. Khezri, T. Marić, N. J. Ch and M. Pumera, *Adv. Funct. Mater.*, 2017, **27**, 1702338.
- 20 A. D. Taboada, L. Maillet, J. H. Banoub, M. Lorch, A. S. Rigby, A. N. Boa, S. L. Atkin and G. Mackenzie, *J. Mater. Chem. B*, 2013, **1**, 707–713.
- 21 T. F. Fan, S. Xiang, L. Li, X. W. Xie, A. L. Chai, Y. X. Shi, N. Liu, R. Abdukerim, J. Y. Ma, J. Shiand and Y. Y. Luan, *Appl. Mater. Today*, 2022, **27**, 101454.
- 22 S. Barri, A. S. Rigby, A. D. Taboada, M. J. Thomasson, G. Mackenzie and S. L. Atkin, *Food Sci. Technol.*, 2010, **43**, 73–76.
- 23 J. Brooks and G. Shaw, *Grana*, 1978, **17**, 91–97.
- 24 Y. Wang, T. Len, Y. Huang, A. D. Taboada, N. B. Andrew, C. Ceballos, F. Delbecq and G. Mackenzie, *ACS Sustainable Chem. Eng.*, 2017, **5**, 392–398.
- 25 H. M. Song, Q. Wei, Q. K. Ong and A. Wei, *ACS Nano*, 2010, **4**, 5163–5173.
- 26 C. L. Nehl, H. Liao and J. H. Hafner, *Nano Lett.*, 2006, **6**, 683–688.
- 27 F. Hao, C. L. Nehl, J. H. Hafner and P. Nordlander, *Nano Lett.*, 2007, **7**, 729–732.
- 28 M. Li, J. W. Kang, R. R. Dasari and I. Barman, *Angew. Chem.*, 2014, **126**, 1–6.
- 29 B. Becerril-Castro, I. Calderon, N. Pazos-Perez, L. Guerrini, F. Schulz, N. Feliu, I. Chakraborty, V. Giannini, W. J. Parak and R. A. Alvarez-Puebla, *Analysis Sensing*, 2022, **2**, e202200005.
- 30 R. He, Y. C. Wang, X. Wang, Z. Wang, G. Liu, W. Zhou, L. Wen, Q. Li, X. Wang, X. Chen, J. Zeng and J. G. Hou, *Nat. Commun.*, 2014, **5**, 4327.
- 31 L. Bazán-Díaz, R. Mendoza-Cruz, J. J. Velázquez-Salazar, G. Plascencia-Villa, D. Romeu, J. Reyes-Gasga, R. Herrera-Becerra, M. José-Yacamán and G. Guisbiers, *Nanoscale*, 2015, **7**, 20734–20742.
- 32 J. J. Velázquez-Salazar, L. Bazán-Díaz, Q. Zhang, R. Mendoza-Cruz, L. Montañó-Priede, G. Guisbiers, N. Large, S. Link and M. José-Yacamán, *ACS Nano*, 2019, **13**, 10113–10128.
- 33 Q. Y. Liu, Y. Zhong, Z. Z. Jiang, K. Chen, S. Ma, P. F. Wang, W. Wang, L. Zhou, M. D. Luoshan and Q. Q. Wang, *J. Mater. Chem. C*, 2020, **8**, 4869–4875.



- 34 Q. Yu, T. Peng, J. Zhang, X. Liu, Y. Pan, D. Ge, L. Zhao, F. Rosei and J. Zhang, *Small*, 2022, **18**, 2103174.
- 35 V. N. Paunov, G. Mackenzie and S. D. Stoyanov, *J. Mater. Chem.*, 2007, **17**, 609–612.
- 36 V. Aylanc, A. F. Peixoto, N. Vale, C. Freire and M. Vilas-Boas, *Appl. Mater. Today*, 2023, **33**, 101860.
- 37 M. J. Uddin, S. Liyanage, J. Warzywoda, N. Abidi and H. S. Gill, *Langmuir*, 2022, **38**, 2763–2776.
- 38 T. Baran, I. Sargin, M. Kaya, A. Menteş and T. Ceter, *J. Colloid Interface Sci.*, 2017, **486**, 194–203.
- 39 F. S. Li, P. Phyto, J. Jacobowitz, M. Hong and J. K. Weng, *Nat. Plants*, 2019, **5**, 41–46.
- 40 P. J. Schouten, D. Soto-Aguilar, A. Aldalbahi, T. Ahamad, S. Alzahly and V. Fogliano, *Curr. Opin. Food Sci.*, 2022, **44**, 100809.
- 41 R. C. Mundargi, M. G. Potroz, J. H. Park, J. Seo, E. L. Tan, J. H. Lee and N. J. Cho, *Sci. Rep.*, 2016, **6**, 19960.
- 42 Y. Duan, X. Liu, L. Han, S. Asahina, D. Xu, Y. Cao, Y. Yao and S. Che, *J. Am. Chem. Soc.*, 2014, **136**, 7193–7196.
- 43 F. Xiang, B. Li, P. Zhao, J. Tan, Y. Yu and S. Zhang, *Adv. Synth. Catal.*, 2019, **361**, 5057–5062.
- 44 R. B. N. Baig and R. S. Varma, *Green Chem.*, 2012, **14**, 625–632.
- 45 D. Clarisse, P. Prakash, V. Geertsens, F. Miserque, E. Gravel and E. Doris, *Green Chem.*, 2017, **19**, 3112–3115.
- 46 Y. Bai, X. Feng, H. Xing, Y. Xu, B. K. Kim, N. Baig, T. Zhou, Y. Lu, E. Oldfield and S. C. Zimmerman, *J. Am. Chem. Soc.*, 2016, **138**, 11077–11080.
- 47 S. Pan, S. Yan, T. Osako and Y. Uozumi, *ACS Sustainable Chem. Eng.*, 2017, **5**, 10722–10734.
- 48 M. Tajbakhsh and M. R. N. Jamal, *Sci. Rep.*, 2022, **12**, 4948.
- 49 L. Bahsis, H. B. E. Ayouchia, H. Anane, A. P. Álvarez, G. D. Munno, M. Julve and S. E. Stiriba, *Appl. Organomet. Chem.*, 2019, **33**, 4669.
- 50 N. Aflak, H. B. E. Ayouchia, L. Bahsis, E. M. E. Mouchtari, M. Julve, S. Rafqah, H. Anane and S. E. Stiriba, *Front. Chem.*, 2019, **7**, 81.
- 51 X. Cai, J. Nie, C. Lu, F. Wang, C. Ma, G. Yang, Z. Chen and Y. Zhang, *Microporous Mesoporous Mater.*, 2021, **310**, 110671.
- 52 S. E. Stiriba, L. Bahsis, E. Benhadria, K. Oudghiri, M. Taourirte and M. Julve, *Int. J. Mol. Sci.*, 2023, **24**, 9301.
- 53 B. Movassagh and N. Rezaei, *Tetrahedron*, 2014, **70**, 8885–8892.
- 54 B. H. Mandal, L. Md. Rahman, M. M. Yusoff, K. F. Chong and S. M. Sarkar, *Carbohydr. Polym.*, 2017, **156**, 175.
- 55 N. Sun, Z. Yu, H. Yi, X. Zhu, L. Jin, B. Hu, Z. Shen and X. Hu, *New J. Chem.*, 2018, **42**, 1612–1616.
- 56 V. Gowri, S. Kumari, R. Sharma, A. Selim and G. Jayamurugan, *ChemRxiv* 2024, DOI: [10.26434/chemrxiv-2024-z93sj](https://doi.org/10.26434/chemrxiv-2024-z93sj).